Two-Way Coupled Eulerian–Eulerian Simulations of a Viscous Snow Phase with Turbulent Drag

Ziad Boutanios and Hrvoje Jasak

Abstract A novel two-way coupled Eulerian–Eulerian CFD formulation was developed to simulate drifting snow based on turbulent drag and a new viscous treatment of the drifting snow phase, derived from first principles. This approach allowed explicit resolution of the saltation layer without resorting to empiricism, unlike other Eulerian–Eulerian models based on mixture formulations and one-way coupling. Initial validations were carried out against detailed snow flux, airflow velocity, and turbulent kinetic energy measurements in a controlled experimental simulation of drifting snow in a wind tunnel using actual snow particles. The two-way coupled approach was found capable of simulating drifting snow fluxes in both saltation and suspension layers with reasonable accuracy. Recommendations were made to improve the accuracy of the method for air velocity and turbulent kinetic energy, and to allow simulating a drifting snow phase with a particle size distribution.

Keywords Drifting snow · Eulerian–Eulerian · Viscosity · Turbulent drag · Snow flux

1 Introduction

Drifting snow results from the aeolian motion of snow particles deposited on the ground. Such motion is possible when the drag force induced by the airflow exceeds the opposing actions of interparticle cohesive bonding, particle weight, and surface friction. This aerodynamic entrainment threshold is called the *fluid threshold*. If a large enough amount of particles is displaced by the airflow it can extract enough momentum from it that the airflow velocity is noticeably reduced; a two-way cou-

---

Z. Boutanios (✉)
Binkz Inc, Laval, Canada
e-mail: ziad@binkz.ca

Z. Boutanios · H. Jasak
Faculty of Mechanical Engineering and Naval Architecture,
University of Zagreb, Zagreb, Croatia
e-mail: hrvoje.jasak@fsb.hr

J. M. Nóbrega and H. Jasak (eds.), *OpenFOAM*®,
https://doi.org/10.1007/978-3-319-60846-4_35

pling phenomenon. Particle collisions also help sustain drifting by putting snowbed particles in motion and making it easier for the slower airflow to carry them at a lower threshold shear stress referred to as the *impact threshold*. Both definitions were first coined by Bagnold [1] in his investigations of desert sand transport by the wind. Bagnold also classified the aeolian motion of particles under three modes: creeping, saltation, and suspension. These modes are shown in Fig. 1 as they pertain to drifting snow. Of particular interest to this research is the two-way coupled saltation mode. Several aeolian snow transport models are available in the literature. Most are based on Reynolds-Averaged Navier–Stokes (RANS) formulations in the Eulerian–Eulerian and Eulerian–Lagrangian frames regarding the air and snow phases, respectively. Both approaches can yield reasonable results for particle-laden flows, but the Eulerian–Eulerian approach requires a lower computational effort since a lot of particles are required for Lagrangian particle tracking to yield statistically meaningful results [2]. Presently, Eulerian–Eulerian modeling of drifting snow is based on two main approaches: the transport of snowdrift density approach and the Volume of Fluid (VOF) approach.

The snowdrift density approach solves a one-way coupled Partial Differential Equation (PDE) for the drifting snow density in the suspension layer (where the snow phase motion does not affect the airflow, a valid assumption in the suspension layer thanks to the very low snow phase concentration) in addition to the airflow continuity and momentum equations with a Prandtl mixing layer model [3]. Another variation of the transport of snow density approach uses the mixture continuity and momentum equations with a standard k–ϵ turbulence model corrected for turbulence damping by particles [4]. Note that the mixture formulation of Naaim et al. [4] is in reality two-way coupled. However, the snow phase momentum equation is not solved. Instead, the snow velocity is set equal to a terminal velocity derived from empirical and experimental considerations. This effectively fixes the two-way coupling effects and the results are indeed quite comparable to other one-way coupled approaches

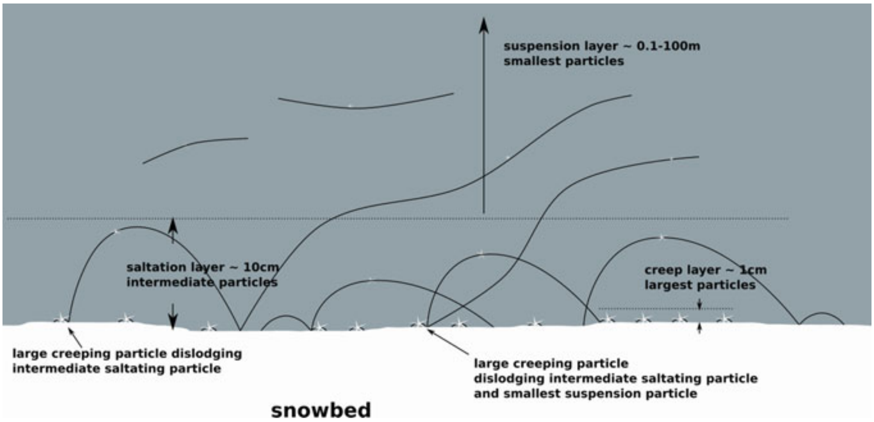

Fig. 1 The different modes of drifting snow

discussed in this section. Another application of the snowdrift density approach uses the airflow continuity and momentum equations with a modified Launder–Kato k–ϵ turbulence model [5]. The drifting snow density is transported by the airflow, the snowfall velocity is set constant, and the saltation layer, which is not resolved, is represented by a steady-state empirical formulation of the transport rate of drifting snow in the saltation layer for equilibrium conditions over natural flat terrain [6]. However, this empirical representation of the saltation layer has been experimentally shown to overestimate the transport rate of drifting snow in accelerating and decelerating flows [7]. This makes such a representation of the empirical layer at best conservative for flows around bluff bodies where important regions of accelerating and decelerating flows are present. The snowdrift density approach with the Launder–Kato turbulence model has been lately modified to account for snow particle damping of turbulence and with saltation computed with the snowdrift density one-way coupled transport equation, without the empirical saltation flux relationships [8]. These modifications resulted in some improvement, but substantial deviations remain from experimental measurements of the snow surface in the lateral vicinity of a cube structure, where accelerating and decelerating effects of bluff body aerodynamics dominate. The computation overestimates the snow accumulation in the stagnation zone ahead of the cube where the flow is reasonably steady state, and is quite good behind it but the simulation authors wonder whether accumulation behind the cube is due to snowfall or snowdrift.

The VOF approach is a one-way coupling interface capturing method that treats the snow phase as a fluid and relies on the assumption that the fluids are not interpenetrating. Capturing of the interface between the phases is done by solving a continuity equation of one or more of the phases, in addition to the mixture continuity and momentum equations. The relative velocity of both phases is based on drift-flux theory, which assumes low drift [9], a reasonable assumption for smaller particles. The VOF approach relies on the same steady-state empirical equilibrium saltation flux treatment as the transport of snowdrift density approach and both methods are equivalent. Different attempts at improving the VOF approach by accounting for particle impingement in saltation as well as modifications of the turbulent wall function roughness parameter based on experiment-specific measurements did not show much improvement compared to experiment, especially close to bluff bodies where accelerating and decelerating flows dominate [10]. No decisive improvement was seen either by using mesh adaptation based on the balance of the convected horizontal snow flux and flow divergence at the ground [11]. Yet another application of the VOF approach uses two different snow phase continuity equations, one with mass diffusion and a suspension particle settling velocity in the suspension layer and another without mass diffusion and a saltation particle settling velocity in the saltation layer [12]. The implementation is based on ad hoc empirical coefficients and parameters, and does not improve on the previously mentioned limitations.

An exception to both approaches above is the physically based one by Gauer [13], which resolves the saltation layer but still uses considerable parameterization and self-similarity assumptions between the airflow profile and the snow concentration profile in the saltation layer, which does not necessarily hold true in the vicinity of bluff bodies. In particular, the air velocity and snow concentration profiles in the saltation layer are assumed and related to the air velocity on top of the saltation layer obtained from the suspension layer computation. The simulations manage to capture the general trends in comparison to experimental snowdrift rates, wind field velocity, and new snow depth for an Alpine crest with order of magnitude agreement in qualitative comparisons. In all fairness, much of the discrepancies are due to poor terrain accuracy and large uncertainty in choosing the correct numerical boundary conditions, as pointed out by the author of the simulations, but the results are inconclusive nonetheless.

The objective of this paper is to present a viable snow phase viscosity model for high rates of strain and two-way coupled situations such as snow saltation, in Eulerian–Eulerian simulations of drifting snow. The viscosity model is implemented in a modified version of `twoPhaseEulerFoam` [14], the formulation of which is based on the following conditional ensemble-averaged equations of conservation of mass and linear momentum used to represent interpenetrating phases in the Gosman model [15]:

$$\frac{\partial \alpha_i}{\partial t} + \nabla \cdot \left(\alpha_i \mathbf{u}_i\right) = 0, \tag{1}$$

$$\frac{\partial}{\partial t}\left(\alpha_i \mathbf{u}_i\right) + \nabla \cdot \left(\alpha_i \mathbf{u}_i \mathbf{u}_i\right) + \nabla \cdot \left(\alpha_i \mathbf{R}_i\right) = -\frac{\alpha_i}{\rho_i}\nabla p + \alpha_i \mathbf{g} + \frac{\mathbf{M}_i}{\rho_i}. \tag{2}$$

Here, α_i, ρ_i, $\mathbf{u}_i$, and $\mathbf{R}_i$ are the volume fraction, density, velocity, and stress tensor of phase i, respectively; p is the static pressure field; and $\mathbf{g}$ is the gravitational acceleration vector; $\mathbf{M}_i$ is the momentum exchange term between the phases,

$$\mathbf{M}_i = \mathbf{F}_l + \mathbf{F}_d + \mathbf{F}_t. \tag{3}$$

Here, $\mathbf{F}_l$, $\mathbf{F}_d$, and $\mathbf{F}_t$ are, respectively, the aerodynamic lift, generalized drag, and turbulent drag forces. Using scale analysis, [13] found the aerodynamic lift and drag forces to dominate at the onset of drifting, but did not consider the turbulent drag force. An earlier scale analysis by [15] including the turbulent drag force found the lift to be negligible for gas/solid particle-laden flows, where the ratio of continuous gas density to dispersed solid density is proportional to 10^{-3}. The lift force is given by

$$\mathbf{F}_l = \alpha_2 \alpha_1 (\alpha_2 C_{ls} \rho_2 + \alpha_1 C_{la} \rho_1) \mathbf{U}_{rel} \times \nabla \times \mathbf{U}. \tag{4}$$

Here, the snow phase is represented by index 1 and the air phase by index 2. $\mathbf{U}_{rel} = \mathbf{U}_2 - \mathbf{U}_1$ is the relative velocity between the phases, and $\mathbf{U} = \alpha_2 \mathbf{U}_2 + \alpha_1 \mathbf{U}_1$ is the mixture velocity. Numerical tests with the present model confirmed the lift force to be negligible; therefore, it was not used in the present simulations. The only two forces found relevant for saltation and suspension are then the generalized aerodynamic and turbulent drag forces. The latter force was also reported to be the main mechanism for transporting smaller particles into suspension [1]. The generalized aerodynamic drag model used is the Gidaspow–Schiller-Naumann model [16], which is expressed as follows for the snow phase:

$$\mathbf{F_d} = K\mathbf{U}_{rel}, \tag{5}$$

$$K = \frac{3}{4d_p}\rho_2 C_D \alpha_2^{-1.65}(1-\alpha_2)|\mathbf{U}_{rel}|. \tag{6}$$

Here, C_D is the drag coefficient on a single sphere given by the following relationship [17]:

$$C_D = \begin{cases} \frac{24}{Re_p}(1+0.15Re_p^{0.687}) & \text{if } Re_p < 1000, \\ 0.44 & \text{if } Re_p \geq 1000. \end{cases} \tag{7}$$

Re_p is the particle Reynolds number based on the particle diameter d_p and air kinematic viscosity ν_2,

$$Re_p = \frac{\alpha_2|\mathbf{U}_{rel}|d_p}{\nu_2}. \tag{8}$$

The Gidaspow–Schiller-Naumann drag model is valid for dilute flows with $\alpha_2 > 0.8$ [18], which is the case in the creep, saltation, and suspension layers. Moreover, the Gidaspow–Schiller-Naumann drag model applies to spherical particles and is used here since no practical correlations for irregular particles as depicted in Fig. 4 are available in the literature. However, as the present irregular particles drift they will rotate around three axes within a somewhat spheroidal volume of air. Therefore, their drag function could be similar to that of a spherical particle with differences that cannot be predicted at the moment. It remains that the spherical particle drag correlations are the only present recourse.

For the snow phase, the turbulent component of the drag force, arising from turbulent fluctuations of the volume fractions and velocities in the Gosman two-fluid model is given by

$$\mathbf{F_t} = -K\frac{\nu^t}{\sigma_\alpha}\nabla\alpha_1. \tag{9}$$

Here, ν^t and σ_α are, respectively, the turbulent kinematic viscosity of the air phase and the Schmidt number. The standard formulation of `twoPhaseEulerFoam` does not include the turbulent drag term. Instead, it uses the continuity equation in the following form:

$$\frac{\partial\alpha_i}{\partial t} + \nabla\cdot(\mathbf{U}\alpha_i) - \nabla\cdot(\mathbf{U}_{rel}\alpha_i(1-\alpha_i)) = 0. \tag{10}$$

Equation 10 provides tighter coupling between the phases since it uses the mixture and relative velocities, as well as both volume fractions [19]. It does not include a turbulent diffusion term, but the third term on the left-hand side can be considered a volumetric mass flow rate source term, playing the same role as a turbulent diffusion term, and a similar role to the turbulent drag term in the momentum equation. For the present simulations, the turbulent drag term of Eq. 9 was added to `twoPhaseEulerFoam`, while retaining the treatment of Eq. 10. The standard incompressible k–ϵ turbulence model is used unmodified and applied only to the air phase, so the interaction between the snow phase and turbulence is not directly taken into account.

The viscous stresses terms in the momentum equations are modeled according to the Boussinesq formulation, which requires a viscosity parameter readily available for air but not for snow. Many snow compactive viscosity models are available for very low rates of strain typical of settling snow, the latest by Teufelsbauer [20] who also provides a review of the main models in the literature. However, nothing is available at the high rates of strain of drifting snow. The next section discusses the high rate of strain viscosity model and its derivation, while the validation of the formulation is presented in the Validationsection. The relevant details of the controlled drifting snow experiment are presented in the Validation Experiment subsection. The numerical setup is presented in the Simulation Setup subsection, followed by the Results and Discussion subsection. The paper concludes with the Conclusionssection which includes recommendations for future work.

2 The Drifting Snow Viscosity Model

The snow phase viscosity is derived by matching the momentum of a number of ideal spherical drifting particles within a control volume, with the momentum of the same control volume containing an equal amount of the equivalent viscous fluid. Drifting snow particles move in transient hops and bounce over the snowbed surface. However, drifting snow can easily be observed in self-sustained steady-state mode in natural and controlled environments, so the motion of the spherical particles can be considered steady state *in the average sense*. This approximation is only used for the purpose of deriving an expression of the snow phase Newtonian viscosity model. A scale analysis showed that the rolling friction force is negligible compared to the drag force, so the former was not retained in the analysis. Neglecting friction forces is further justified by the fact that their effects and that of snowbed asperities are already implicitly included in the surface threshold shear–stress parameter.

The derivation starts with the momentum equations of the air and snow phase for fully developed steady-state flow in a control volume containing a number of rolling particles on the snowbed and having the same height as a particle. At typical drifting snow particle height $d_p \leqslant 1\,\text{mm}$, typical surface threshold friction velocity $u_* \leqslant 0.5$ [21] and air temperature below freezing, the nondimensional wall distance to the snowbed is $y_+ \leqslant 50$. Under such conditions the airflow profile is weakly nonlinear and the divergence of the stress tensor negligible compared to the pressure gradient. Therefore, we can write the snow and air momentum equations for steady-state fully developed flow as

$$-\alpha_1 \frac{\partial P}{\partial x} + F_d + \alpha_1 \mu_1 \frac{d^2 u_1}{dy^2} = 0, \tag{11}$$

$$-\alpha_2 \frac{\partial P}{\partial x} - F_d = 0. \tag{12}$$

Here, $\partial P/\partial x$ is the downstream pressure gradient, F_d is the drag force on a particle and μ_1 is the snow phase dynamic viscosity. One can eliminate the drag force between the equations above and solve for the snow phase velocity on the snowbed using the following no-slip and threshold shear stress boundary conditions at the snowbed surface:

$$u_1 = 0, \tag{13}$$

$$\tau_t = \alpha_2 \rho_2 u_*^2. \tag{14}$$

The resulting snow phase velocity on the snowbed is

$$u_1(y) = \frac{1}{2\alpha_1 \mu_1} \frac{\partial P}{\partial x} y^2 + \frac{\tau_t}{\alpha_1 \mu_1} y. \tag{15}$$

The expression for the dynamic viscosity is obtained by matching the linear momentum of the Lagrangian snow particle phase with that of the equivalent Eulerian snow fluid phase. The Lagrangian linear momentum per unit volume $P_{L,v}$ is given by Eq. 16, where ρ_i is the ice density and V_p the average particle velocity. The Eulerian linear momentum per unit volume $P_{E,v}$ is given by Eq. 17.

$$P_{L,v} = \alpha_1 \rho_i V_p, \tag{16}$$

$$P_{E,v} = \alpha_1 \rho_i d_p \int_0^{d_p} u_1(y) dy. \tag{17}$$

Integrating and setting $P_{L,v} = P_{E,v}$ provides the following expression of the drifting snow dynamic viscosity:

$$\mu_1 = \frac{\frac{1}{6} \frac{\partial P}{\partial x} d_p + \frac{1}{2} \tau_t}{\dot{\gamma}_1}. \tag{18}$$

Here, $\dot{\gamma}_1 = \alpha_1 \dfrac{V_p}{d_p}$ is the particle phase rate of strain. Equation 18 can also be reformulated in terms of the drag force,

$$\mu_1 = \frac{-\frac{1}{6}\dfrac{F_d d_p}{\alpha_2} + \frac{1}{2}\tau_t}{\dot{\gamma}_1}. \tag{19}$$

In aeolian transport phenomena particles, the drag force usually points downstream, in the direction of the decreasing downstream pressure gradient. On the other hand, the surface shear stresses usually resist the particle motion, and this competition between the threshold shear stress τ_t and the pressure gradient (or drag force) is highlighted in Eqs. 18 and 19. The pressure gradient and the drag force tend to induce motion, reducing the effective viscosity of the snow phase, whereas surface shear stresses tend to inhibit motion, increasing the effective viscosity of the snow phase. Within the snowbed, the snow Eulerian continuum should still be characterized by the threshold shear stress. Since there is no significant airflow beneath the snow surface, and we are not interested in an accurate simulation of snowbed packing, the drag/pressure gradient term can be eliminated from Eqs. 18 and 19 in that region. The resulting drifting snow viscosity expression implemented and tested here is the following:

$$\mu_1 = \begin{cases} 0.5\dfrac{\tau_t}{\dot{\gamma}_1} & \text{in snowbed} \\ \left(-\frac{1}{6}\dfrac{F_d d_p}{\alpha_2} + \frac{1}{2}\tau_t\right)/\dot{\gamma}_1 & \text{in creeping, saltation and suspension.} \end{cases} \tag{20}$$

3 Validation

This section presents the relevant details of the controlled wind tunnel drifting snow experiment and the numerical setup. The discussion proceeds around the results of the numerical simulations as compared to the experimental measurements.

3.1 Validation Experiment

The experimental data used to validate the present viscosity model comes from a controlled wind tunnel experiment of drifting snow using actual snow particles [22]. The experiment was carried out at the Cryospheric Environment Simulator (CES) of the Shinjo Branch of the Snow and Ice Research Center (SIRC), at the National Research Institute for Earth Science and Disaster Prevention (NIED) in Japan, by the snow research group of Tohoku University. This experiment was selected because it included detailed measurements of the snow fluxes and airflow velocity profiles at four measurement stations in the working section of the tunnel, and across the

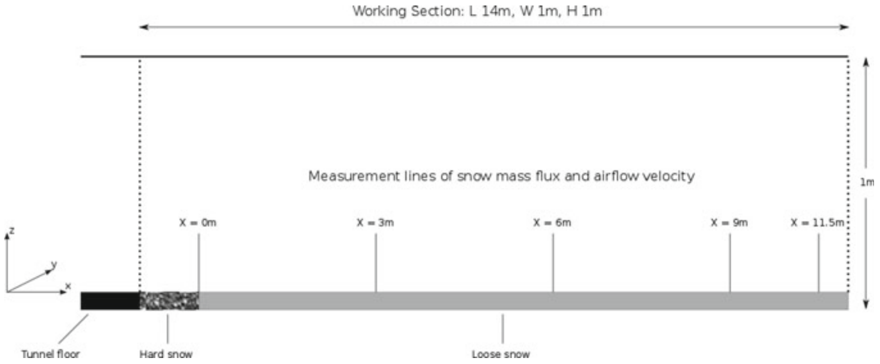

Fig. 2 Side view of the wind tunnel experimental layout (adaptation of Fig. 2 from Okaze et al. [22])

entire saltation layer and lower part of the suspension layer. Turbulent kinetic energy profiles were also measured at the most downstream measurement station.

The experimental layout is shown in Fig. 2 with the locations of the experimental measurement stations. The first measurement station is at $X = 0$ m and is preceded by a 1 m fetch of hardened snow that cannot drift. This induces a nonequilibrium boundary layer before the 14 m working section which includes a 0.02 m deep groove filled with loose snow that can drift. The turbulence kinetic energy and airflow velocity profiles were measured at X = 0 m, and they are shown in Fig. 3. They are nondimensionalized using the reference airflow velocity U_r at a height of 0.2 m over the snowbed. The airflow velocity and snow flux profiles were also measured at the downstream stations located at $X = 3$, 6, 9 and 11.5 m. The turbulent kinetic energy profile was also measured at the last downstream station at $X = 11.5$ m. The experiment was initiated with a start-up phase of 25 s to reach the conditions shown in Fig. 3, followed by a waiting period of 5 s. The airflow velocity, turbulent kinetic energy, and snow flux profiles were then measured at all four downstream stations within a global time window of 30 s, consisting of 5 s for each station and a 2 s transfer period in between stations. The reported results of snow flux, airflow velocity, and turbulent kinetic energy profiles were obtained by averaging the data measured during the individual 7-s windows. The reader is referred to Okaze et al. [22] for the experimental details. Samples of the snow particles used in the experiment are shown in Fig. 4 with a 1 mm scale bar. The experimental snow particles are quite irregular and bulky, exceeding 1 mm in length quite often but rarely smaller than 0.10 mm in either length or width.

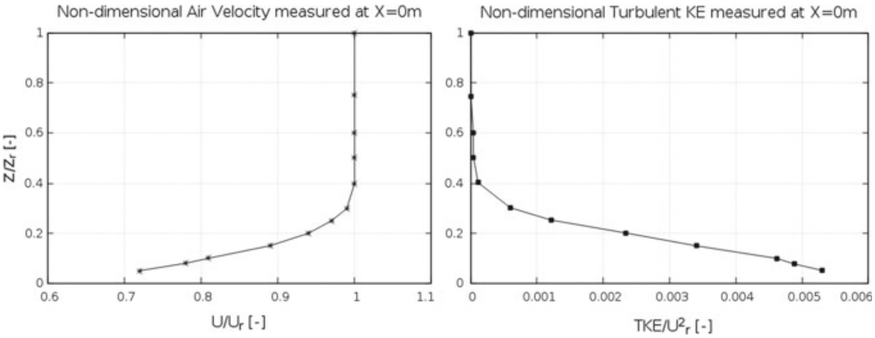

Fig. 3 Experimental airflow velocity and turbulent kinetic energy profiles measured at $X = 0$ (adapted from Fig. 3 of Okaze et al. [22])

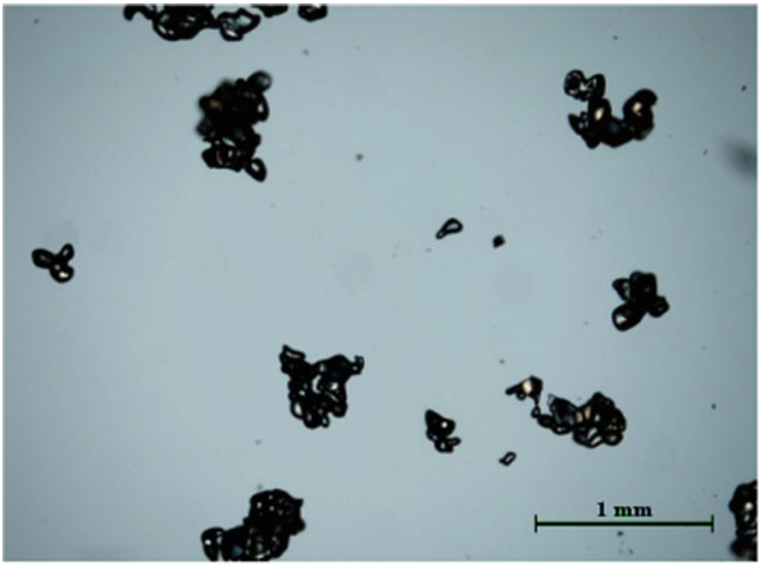

Fig. 4 Samples of the snow particles used in the experiment with a 1 mm scale bar (provided by Dr. Tsubasa Okaze)

3.2 Simulation Setup

The 2D computational mesh used for the simulations is shown in Fig. 5. A close-up of the mesh at the inlet of the computational domain at $X = 0$ m is also shown, with the loose snow layer in the gutter in white. The volume fraction of the snowbed was set to 0.394 in order to match the experimentally measured snowbed density of 361 kg/m^3. The mesh is fully structured, composed of hexahedral elements with a transverse element size of 4 mm in the gutter and at the top of the tunnel. The

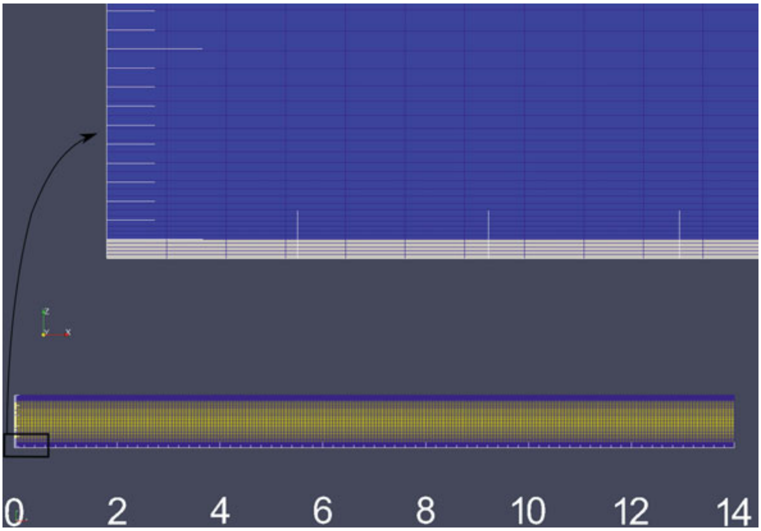

Fig. 5 Simulation mesh with a close-up of the inlet region showing the loose snow layer in the gutter

longitudinal element size in the flow direction along the X-axis is about 6 cm. Tests were carried out with a mesh twice finer in both directions and the results varied by less than 15%, so the results obtained from the present mesh can be reasonably considered mesh-independent.

The `Gauss linear` scheme was used for gradients and divergence of viscous terms, and the `Gauss upwind` scheme for divergence of nonlinear convection terms. The `Gauss linear orthogonal` scheme was used for all Laplacians. The pressure equation was solved with GAMG and DIC smoother, and all other equations were solved with PBiCG and DILU preconditioner. All solvers were converged to ten orders of magnitude. The measured profiles of airflow velocity and turbulent kinetic energy at $X = 0$ m from Fig. 3 were imposed as inlet boundary conditions for the simulations, with a Neumann zero-gradient inlet boundary condition for the pressure. At the inlet, the `turbulentMixingLengthDissipationRateInlet` boundary condition was used for ϵ, which is based on the following equilibrium relationship:

$$\epsilon = \frac{C_\mu^{0.75} k^{1.5}}{l_m}. \tag{21}$$

Here, $C_\mu = 0.09$ is the familiar k–ϵ model constant and l_m is the mixing length set to half the wind tunnel height, or the assumed dimension of the large inertial eddies. Tests were conducted with a mixing length equal to 10% of the wind tunnel height with negligible differences in the results, perhaps due to the low sensitivity of the k–ϵ model to changes in inlet conditions. At the outlet, Neumann zero-gradient boundary conditions were used for all variables except the pressure, with a Dirichlet zero-value boundary condition. Standard wall functions were used at the walls.

Simulations were carried out at a snow threshold shear stress $\tau_t = 0.044\,\mathrm{Kg/(m\,s^2)}$, which is the minimum experimentally observed value for drifting, and corresponds to a threshold velocity of $u_* = 0.23$ m/s. The drifting experiment analyzed here is transient, given the limited supply of drifting snow in the wind tunnel gutter, so the simulations were accordingly carried out in transient mode. Moreover, it is necessary to take into account the particle size distribution when using two-way coupled simulations [23]. The present formulation can only account for one particle size at a time. Therefore, the only way to reproduce the results of a particle size distribution was to combine the results of several single particle size simulations, using the statistical weight of each size class in the distribution. Particle size distributions were not reported in the experimental paper but mechanical breakage phenomena such as drifting snow usually obeyed a two-parameter Gamma distribution be it as aggregate on the ground [24] or drifting above it [25]. The two-parameter Gamma Probability Distribution Function (PDF) $f(x)$ and the Gamma function Γ are expressed as

$$f(x) = \frac{b^a}{\Gamma(a)} x^{a-1} e^{-bx}, \tag{22}$$

$$\Gamma(a) = \int_0^\infty x^{a-1} e^{-x} dx, \qquad a \in (0, \infty). \tag{23}$$

Here, a and b are, respectively, the distribution shape and scale parameters, and they define the distribution average size as $d_{avg} = a/b$. The statistical weight w_i of a particle class d_i is calculated as follows:

$$w_i = \int_{\frac{d_i + d_{i-1}}{2}}^{\frac{d_{i+1} + d_i}{2}} f(x) dx. \tag{24}$$

Here, d_{i-1} and d_{i+1} are the lower and upper particle size classes. The percentage contributions of the different particle classes to several distributions with average particle size of 0.7, 0.8, and 0.9 mm are shown in Fig. 6. In this section, the snow flux and airflow velocity profiles of a two-parameter Gamma distribution with average diameters of 0.7, 0.8, and 0.9 mm are reproduced using all seven particle size simulations, namely, 0.1, 0.3, 0.5, 0.7, 0.9, 1.1, and 1.3 mm particle sizes. The particle size distribution results are then compared to the results of the single diameter distributions from the previous section and the experimental measurements.

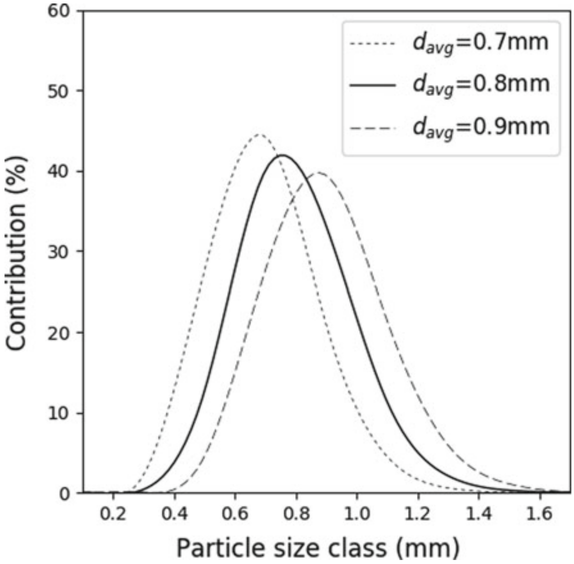

Fig. 6 Percentage contributions of different particle size classes to distributions with d_{avg} = 0.7, 0.8 and 0.9 mm

3.3 Results and Discussion

The average snow flux profiles at X = 11.5 m are shown in Fig. 7, along with the experimental measurements. The numerical profile for the average diameter of 0.7 mm exceeds the experimental measurements by far, especially high in the saltation and suspension layers. This is due to the important contributions of the smallest particles that are most present in that distribution. The smallest and lightest particles are transported in saltation and suspension more easily than the larger particles, which are heavier and tend to drift closer to the snowbed. Accordingly, the distributions with average diameters of 0.8 and 0.9 mm have less contribution from the smallest particles and less saltation/suspension snow flux. The distribution snow flux profiles appear quite sensitive to small changes in the average distribution diameter since the PDF curves in Fig. 6 are pretty narrow and have little spread around the average diameter value. However, all three profiles show a reasonable qualitative agreement with the experimental data since the shapes of the experimental and simulation profiles are similar and the simulation profiles intersect the experimental profile, especially for the 0.9 mm average diameter case.

The profiles of average nondimensional airflow velocity for the same average diameters of 0.7, 0.8, and 0.9 mm are shown in Fig. 8. Again, a reasonable qualitative agreement is found with the experimental measurements since the shapes of all curves are pretty much the same, but with much smaller differences between the three distributions. This implies that the distribution velocity is less sensitive than the distribution snow flux to small changes in the average distribution diameter, for

Fig. 7 Average snow flux profiles at X = 11.5m, for distribution average diameters of 0.7, 0.8, and 0.9 mm

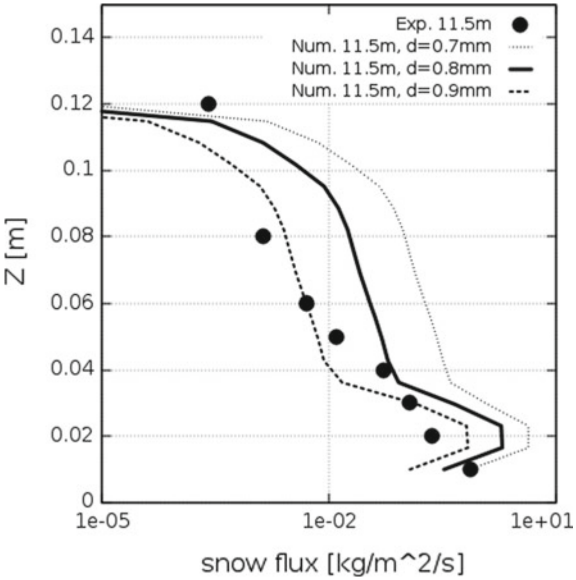

Fig. 8 Average profiles of nondimensional airflow velocity at X = 11.5m, for distribution average diameters of 0.7, 0.8, and 0.9 mm

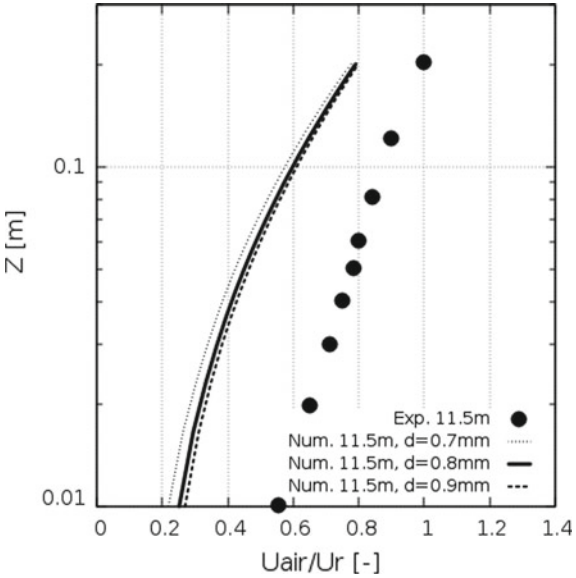

the range of average distribution diameters considered. Therefore, the quantitative differences should not be due to the averaging process.

The average nondimensional turbulent kinetic energy profiles are shown in Fig. 9 and are found to be equally insensitive as the airflow velocity profiles. Moreover, the numerical results exceed the experimental measurements by two orders of magnitude,

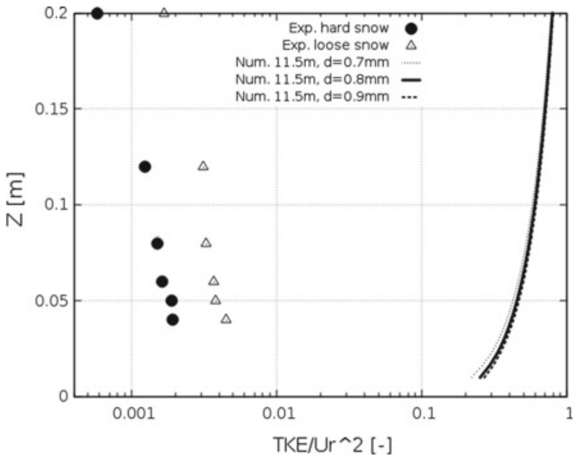

Fig. 9 Average profiles of nondimensional turbulent kinetic energy at X = 11.5m, for distribution average diameters of 0.7, 0.8, and 0.9 mm

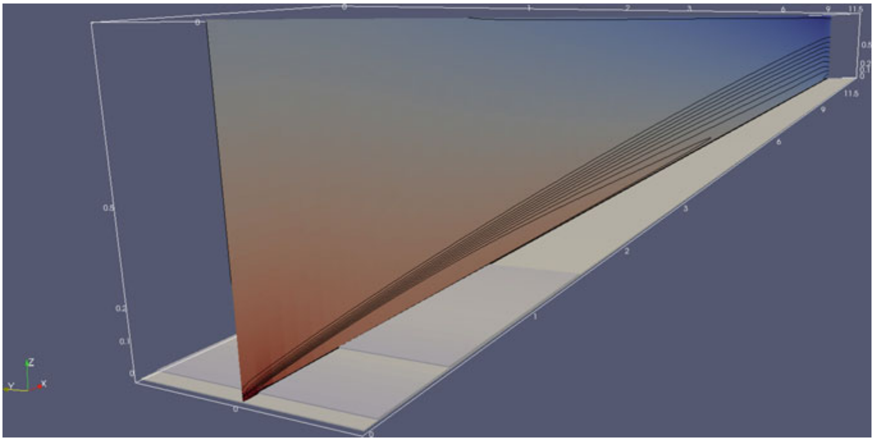

Fig. 10 Pressure stagnation zone forming at the beginning of the eroding snowbed, with turbulent kinetic energy contours

a well-known flaw of the k–ϵ model in stagnation regions [26, 27]. This deficiency is also known to affect downstream parts of the flow [28]. In the present case, the stagnation region is located upstream right after the inlet, where the flow trips into the eroding snowbed as can be seen in Fig. 10. The turbulent kinetic energy contours are also shown in black, and they extend downstream reaching the 11.5 m measurement station. The drifting snow particles constitute another contributing factor since they extract significant momentum from the airflow by drag in the saltation layer. This two-way coupled effect fades away in the suspension layer, where the airflow subsequently accelerates, forming another shear layer where turbulence is also generated [1]. The standard k–ϵ model used here is not equipped to handle such dispersed two-phase flow situations. However, many fixes are available in the literature in the form of turbulent timescale limiters [28] and particle effect source terms in the k and ϵ transport equations [29]. They will be investigated in future work, as well as the specific k–ϵ implementation in `twoPhaseEulerFoam`.

4 Conclusions and Future Work

A new two-way coupled Eulerian–Eulerian formulation to simulating drifting snow was presented along with validation results against a controlled wind tunnel drifting snow experiment. The new formulation was implemented in OpenFOAM®, based on `twoPhaseEulerFoam`. It includes a novel drifting snow viscosity model developed to allow computing the viscous stress tensor in the snow phase momentum equation, which itself made it possible to simulate drifting snow in the saltation layer without resorting to empirical correlations used by other Eulerian methods.

Comparisons of simulation results with experimental measurements showed that the new two-way coupled formulation behaves physically with respect to particle size. The model showed reasonable qualitative agreement with measured snow flux in the saltation and suspension layers. Comparisons of numerical airflow velocity to experiment showed reasonable qualitative agreement with the experimental profiles, with quantitative deficit in the numerical results. These are believed to be due to well-known deficiencies of the standard k–ϵ model, which can be addressed with fixes available in the literature.

The present formulation allows simulating one particle diameter class, and work is ongoing to allow simulating several diameter classes simultaneously. Corrections to the k–ϵ model excess turbulent kinetic energy production are also being implemented. This viscous model can be extended quite easily to aeolian transport of sand and even riverbed sediment transport, to give only a couple of examples.

Acknowledgements The authors warmly thank Profs. Akashi Mochida, Tsubasa Okaze, and Yoshihide Tominaga for sharing their experimental results. In particular, the patience and dedication of Prof. Okaze to answering our numerous questions are gratefully acknowledged. Many thanks!

References

1. R. Bagnold, *The physics of blown sand and desert dunes*. London, Methuen, 1941.
2. B. Lee, J. Tu, and C. Fletcher, “On numerical modeling of particle-wall impaction in relation to erosion prediction: Eulerian versus Lagrangian method,” *Wear*, vol. 252, pp. 179–188, 2002.
3. T. Uematsu, T. Nakata, K. Takeuchi, Y. Arisawa, and Y. Kaneda, “Three-dimensional numerical simulation of snowdrift,” *Cold Regions Science and Technology*, vol. 20, pp. 65–73, 1991.
4. M. Naaim, F. Naaim-Bouvet, and H. Martinez, “Numerical simulation of drifting snow: erosion and deposition model,” *Annals of Glaciology*, vol. 26, pp. 191–196, 1998.

5. Y. Tominaga and A. Mochida, “CFD prediction of flowfield and snowdrift around a building complex in a snowy region,” *Journal of Wind Engineering and Industrial Aerodynamics*, vol. 81, no. 13, pp. 273 – 282, 1999.
6. J. Pomeroy and D. Gray, “Saltation of snow,” *Water Resources Research*, vol. 26, no. 7, pp. 1583–1594, 1990.
7. T. Okaze, A. Mochida, Y. Tominaga, M. Nemoto, Y. Ito, and T. Shida, “Modeling of drifting snow development in a boundary layer and its effect on windfield,” in *The Sixth Snow Engineering Conference*, Whistler, B.C., Canada, June 1–5 2008.
8. Y. Tominaga, T. Okaze, and A. Mochida, “CFD modeling of snowdrift around a building: overview of models and evaluation of a new approach,” *Building and Environment*, vol. 46, pp. 899–910, 2011.
9. B. Bang, A. Nielsen, P. Sundsbø, and T. Wiik, “Computer simulation of wind speed, wind pressure and snow accumulation around buildings (SNOW-SIM),” *Energy and Buildings*, vol. 21, no. 3, pp. 235–243, 1994.
10. J. Beyers, “Numerical modeling of the snowdrift characteristics surrounding the SANAE IV research station,” Ph.D. Dissertation, Department of Mechanical Engineering, University of Stellenbosch, 2004.
11. J. Beyers and B. Waechter, “Modeling transient snowdrift development around complex three-dimensional structures,” *Journal of Wind Engineering and Industrial Aerodynamics*, vol. 96, pp. 1603–1615, 2008.
12. P. Sundsbø, “Numerical simulations of wind deflection fins to control snow accumulation in building steps,” *Journal of Wind Engineering and Industrial Aerodynamics*, vol. 74–76, pp. 543–552, 1998.
13. P. Gauer, “Blowing and drifting snow in alpine terrain: A physically-based numerical model and related field measurements,” Ph.D. dissertation, ETH Zurich, 1999.
14. *OpenFOAM Documentation, Extended Code Guide*, 2018.
15. A. Gosman, R. Issa, C. Lekakou, S. Politis, and M. Looney, “Multidimensional modeling of turbulent two-phase flows in stirred vessels,” *AIChE Journal*, vol. 38, no. 12, pp. 1946–1956, 1992.
16. D. Gidaspow, “Hydrodynamics of fluidization and heat transfer: supercomputer modelling,” *Appl. Mech. Rev.*, vol. 39, pp. 1–22, 1986.
17. L. Schiller and Z. Naumann, “A drag coefficient correlation,” *Z. Ver. Deutsch. Ing.*, vol. 77, 1935.
18. H. Enwald, E. Peirano, and A.-E. Almstedt, “Eulerian two-phase flow theory applied to fluidization,” *Int. J. of Multiphase Flow*, vol. 22, pp. 21–66, 1996.
19. H. Weller, “Derivation, modelling and solution of the conditionally averaged two-phase flow equations,” OpenCFD Ltd, Report TR/HGW/02, 2005.
20. H. Teufelsbauer, “A two-dimensional snow creep model for alpine terrain,” *Natural Hazards*, vol. 56, pp. 481–497, 2011.
21. R. Kind, *Handbook of Snow, Principles, Processes, Management and Use*. Pergamon Press, 1981, ch. Snowdrifting, pp. 338–359.
22. T. Okaze, A. Mochida, Y. Tominaga, M. Nemoto, T. Sato, Y. Sasaki, and K. Ichinohe, “Wind tunnel investigation of drifting snow development in a boundary layer,” *J. Wind Eng. Ind. Aerodyn.*, vol. 104-106, pp. 532–539, 2012.
23. Z. Boutanios and H. Jasak, “Viscous treatment of the snow phase in Eulerian-Eulerian simulations of drifting snow,” in *The 14th International Conference on Wind Engineering*, Porto Alegre, Brazil, June 21-26 2015.
24. W. Budd, “The drifting of nonuniform snow particles,” in *Studies in Antarctic meteorology*, M. Rubin, Ed. American Geophysical Union, 1966.
25. R. Schmidt, “Vertical profiles of wind speed, snow concentration and humidity in blowing snow,” *Boundary-Layer Meteorology*, vol. 23, no. 2, pp. 223–246, 1982.
26. W. Strahle, “Stagnation point flows with freestream turbulence – the matching condition,” *AIAAJ*, vol. 23, pp. 1822–1824, 1985.

27. B. Launder and M. Kato, “Modeling flow-induced oscillations in turbulent flow around square cylinder,” in *ASME Fluid Eng. Conference*, 1993, p. 20.
28. P. Durbin, “Separated flow computations with the k–epsilon-v2 model,” *AIAA Journal*, vol. 33, pp. 659–664, 1995.
29. T. Okaze, Y. Takano, A. Mochida, and Y. Tominaga, “Development of a new $k - \epsilon$ model to reproduce the aerodynamic effects of snow particles on a flow field,” *J. Wind Eng. Ind. Aerodyn.*, vol. 144, pp. 118–124, 2015.